Materials Science Forum
ISSN: 1662-9752, Vol. 1188, pp 57-73

Submitted: 2026-01-19
Revised: 2026-02-22
Accepted: 2026-02-22
Online: 2026-04-20

Additive Manufacturing for Advanced and Functional Tooling of Dies Used in High-Pressure Die Casting Processes

Sri Harini RAJENDRAN[1,a*], Nagasivamuni BALASUBRAMANI[2,b] and Mohamed EL MANSORI[1, c]

[1]Mechanics, Surfaces and Materials Processing Laboratory (MSMP), Arts et Métiers Institute of Technology, Châlons-en-Champagne F-51006, France.

[a*]sri-harini.rajendran@ensam.eu, [b]nagasivamuni.balasubramani@ensam.eu, [c]Mohamed.elmansori@ensam.eu

Keywords: Additive manufacturing, solidification, microstructure, high-pressure die casting

Abstract This article aims to review the recent advances in the laser powder bed fusion process (L-PBF) of H13 tool steel for the dies used in the high pressure die casting (HPDC) applications. The effect of processing variables is briefly reviewed for the evolution of microstructure (phase transformations, as-built microstructure and carbides precipitation), mechanical properties, and defects. The second part of the review is focused on conformal cooling applications to HPDC dies, which is critical for die life and productivity. Achieving better microstructure without defects, understanding the role of processing variables in L-PBF and their interdependencies remains the key challenge for the as-built part, while the benefits of preheating and post-heat treatments are evident. Significant benefits are realized in the applications of die inserts favoring lower die surface temperature, reduced cycle time and lubrication, and thermo-mechanical stresses. In addition, L-PBF also plays a key role in die remanufacturing where significant benefits are achieved in terms of materials savings and improved performance compared to traditional repair technologies. Overall, L-PBF offers a transformative pathway for high-performance HPDC dies; however, most investigations are trial-based. Long-term studies are needed for performance assessment and establishing failure mechanisms in production environments.

Introduction

High-Pressure Die Casting (HPDC) is used to fabricate complex, high-volume, and high-precision metallic components for the automotive, aerospace, and electronics sectors. HPDC makes up roughly 60-70% of the cast alloy market, primarily for automotive applications. A significant growth for the automotive market and lightweight requirements is predicted due to the electrification of vehicles, where large capacity HPDC machines (mega/giga castings) are used in the production of integrated structural castings for front and rear end parts [1,2]. The quality of the produced components is linked to the performance of the dies used in die-casting, which are subjected to extremely severe service conditions, including high forming loads, repeated thermal cycling, intense mechanical stresses, erosion, and wear. Hot working tool steel, H13 (Cr-hot working tool steels) is characterized by excellent resistance to high temperature impact, loading and softening due to thermal fatigue, presence of medium C content and higher Cr with other carbide forming elements. The formation of fine and stable V- and Cr- containing carbides is key to the high temperature strength and hardenability [3]. Dies used in the HPDC process are generally designed for longer operating cycles (~100,000 to 300,000) to reduce repair and maintenance costs. However, most dies fail during service conditions due to heat checking, wear, plastic deformation, die soldering, and corrosion [4]. Cyclic heating and cooling during the casting process induce significant thermal gradient fluctuations, resulting in compression stresses at the surfaces of the mold and tensile stresses during cooling. A steady decrease in the surface hardness is noted after ~6500 cycles, and this softening causes cracks to appear on the surface of the dies, known as heat checks [5]. In addition to thermal loading, cyclic mechanical and tribological loadings lead to wear damage that affects the tool life and dimensions of the part [5]. Conventional dies for HPDC are typically manufactured by machining hot work tool

steels, which restricts the complex geometry of internal cooling channels and limits thermal management capabilities, ultimately shortening the die life. The severity of the die damage determines whether the die can be repaired by welding for further use or must be recycled [6]. Several approaches, such as surface treatments and improved thermal management during the HPDC process, are adopted to extend die life; however, achieving effective thermal control to improve die life remains a critical challenge. Thermal fatigue accounts for nearly 70% of the casting die failures and 30% of production costs [7].

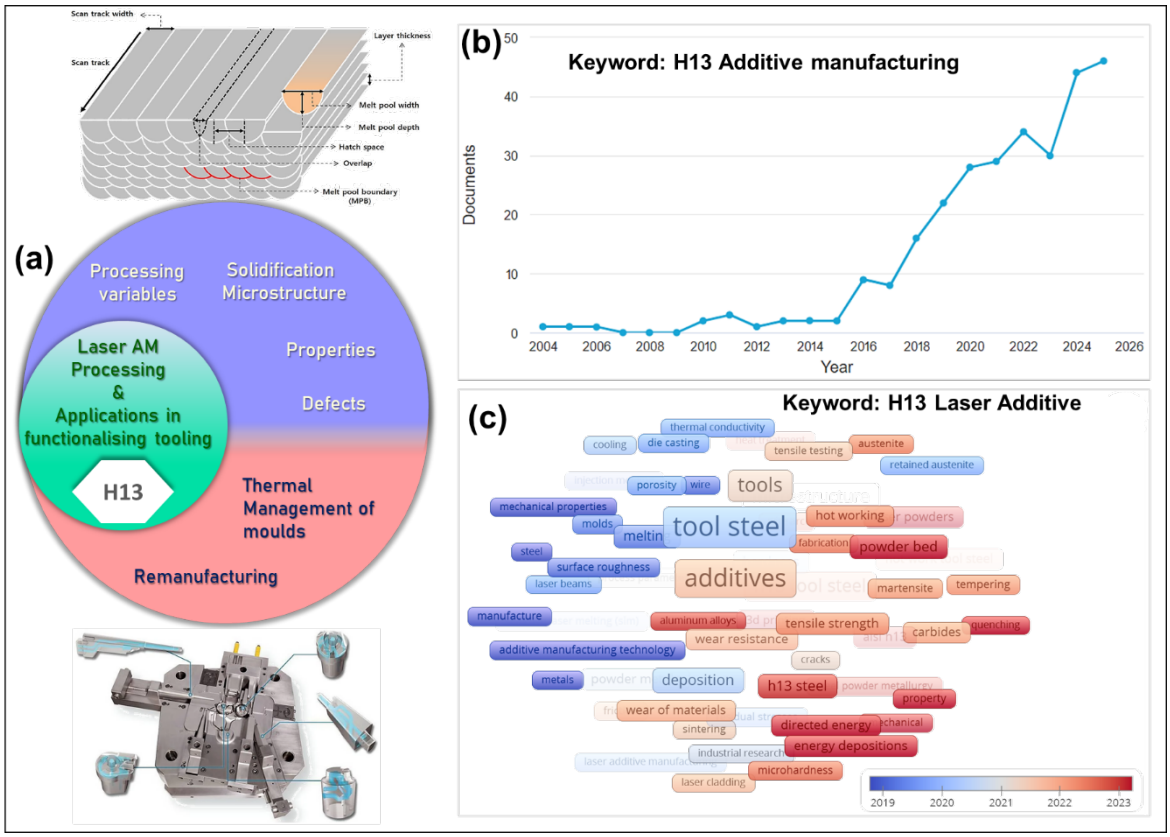

Fig. 1 (a) Overview of the review paper highlighting the important process variable and applications [8,9] (b) publications per year and (c) indexed keywords from the Scopus database for H13 tool steels.

Additive manufacturing (AM), especially laser and electron beam powder bed fusion (L-PBF and E-PBF) processes, also referred to as Selective Laser Melting (SLM) or Laser Beam Melting (LBM), Direct Metal Laser Sintering (DMLS), and Electron Beam Melting (EBM) [10,11], offers greater potential. Originally developed for rapid prototyping and tooling, they have gained significant interest in recent years for promoting integrated and circular manufacturing solutions. For the HPDC industry, AM of tool steels provides significant advantages in the production of mold inserts, supporting repair and remanufacturing [6]. Notably, AM enables the fabrication of dies with conformal cooling channels, which are otherwise constrained by the limited design freedom of conventional processes [12]. Reducing the local hotspot regions within the mold, improving homogeneity or controlled cooling (directed solidification), reducing the propensity for defects and cycle time. Besides, die surface temperature reduction is critical to reduce the consumption of lubricants or die releasing agents [13,14]. AM also supports lattice reinforcements and multi-material gradients, offering localized tailoring of properties and reducing material costs [15]. Since AM facilitates seamless integration with simulation-based optimization, designers can develop and optimize application-specific tooling and integrated process–structure–property–performance (PSPP) modelling [16]. Although L-PBF processes enabled significant advances, such as improved part density, build rates, and the integration of conformal cooling, challenges such as residual stress, cracking, and the high surface roughness of PBF channels affect flow behaviour and heat transfer [8]. The most common

challenges are (i) achieving uniform microstructure, (ii) better mechanical properties, (iii) part density without defects (porosity, lack of fusion, cracks), and (iv) optimising heat treatment conditions [17].

Fig. 1a highlights an overview of the article focusing on the microstructure and applications of H13 tool steel (related tool steels used for mold inserts) fabricated by L-PBF applied to the HPDC process. A broad keyword search using Scopus is performed for the keywords "H13 and additive manufacturing," which yielded 293 results from 2004-2025 as shown in Fig. 1b. This unfiltered keyword search is further plotted for the number of appearances over years as shown in Fig. 1c. The keyword search mainly highlights the number of keyword appearances over the years that are mainly limited to processing methods, microstructure, and properties. These documents were manually assessed and found that there are continued interests to examine the effects of process parameters (not limited to deposition strategy, energy input, scan speed, hatch spacing), defects, heat treatments, preheating, surface modification, powder characteristics, alloying elements, mechanical and fatigue properties, mold repair and remanufacturing. Since recent reviews have extensively focused on investigating the role of process variables in detail for H13 tool steel, this review is intended to highlight only the main observations of the current status. Therefore, this review is divided into two main parts, where the first section is aimed at summarizing the key findings for the process parameters and highlighting the recent research works on the microstructure, defects, mechanical properties, and the role of heat treatment, since several research articles recently covered these topics extensively [4,11,15,17]. The second part of the review is aimed at reviewing the application of additively manufactured H13 tool steels in casting dies, which is relatively less explored and addresses the current progress, potential opportunities, and outstanding challenges, including the scope for remanufacturing processes.

Additive manufacturing of tool steels

The factors that directly influence the robustness of additive manufactured H13 parts can be broadly classified as process parameters, powder metallurgy considerations, and post-processing treatments, each governing the microstructure evolution, residual stress development, and defect formation, which together determine the thermal and mechanical properties [17]. A review by Wu et al. [11] classified these parameters into material-dependent and material-independent parameters as shown in Fig. 2. The first group includes powder quality, laser/machine settings, and post-heat treatments. Part geometry (CAD model, slicing) and process preparation (operational, environmental, and other variables) are the main components of the second group.

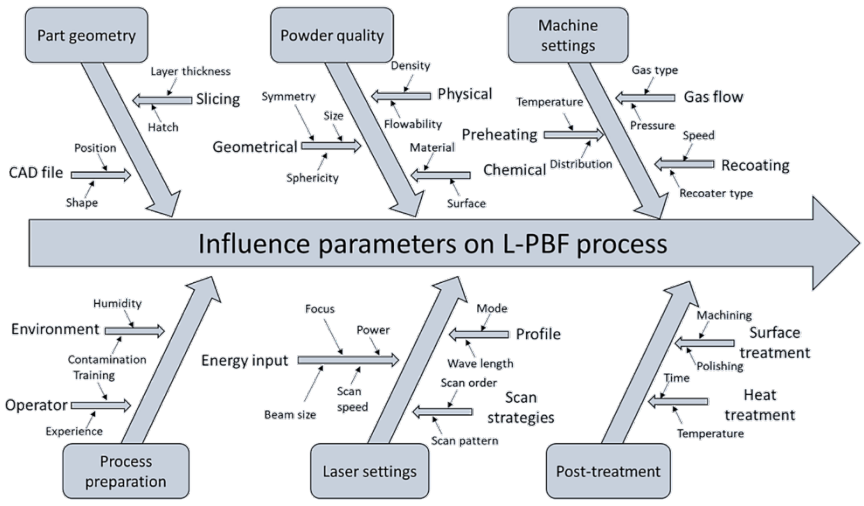

Fig. 2 Factors influencing the part quality in the L-PBF process [11].

In this section, the focus is placed on two key aspects of AM: the role of process parameters, effects of heat treatment, and residual stress. Optimizing these material-dependent variables is essential, as they directly influence the performance, reliability, and service life of tool steel dies.

Role of process parameters on microstructure and defects

Fabricating of H13 parts in AM without defects is challenging due to the complex interactions between the processing parameters and the resultant microstructure. In AM components, defects and microstructure are closely interconnected as both evolve under the same thermal cycles, energy input, and melt pool dynamics inherent to the layer-by-layer fabrication process.

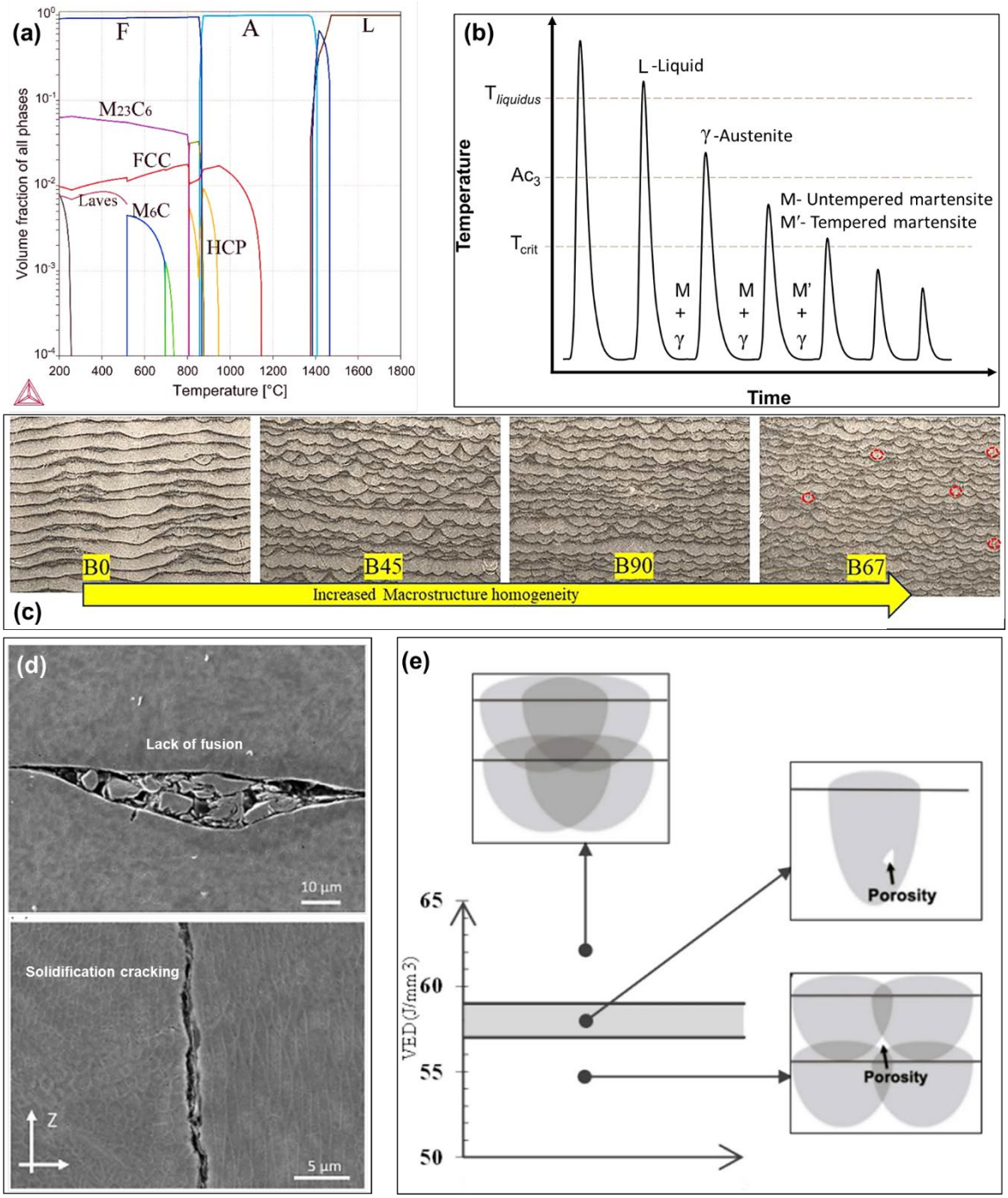

Fig. 3 (a) Isopleth phase diagram of H13 tool steel [20], (b) phase transformations during L-PBF of tool steel [21], (c) bidirectional scan strategy with different rotational angles (0, 45,90, 67°) showing macrostructure homogeneity [22], (d) lack of fusion and solidification cracking [11], and (e) porosity map as a function of energy density [23].

Porosity, lack of fusion, incomplete melting, hot cracks, and solidification cracks are the common defects. Porosities with irregular morphologies primarily form because of incomplete fusion, while spherical porosities could be due to gas entrapment, both of which can act as stress concentration sites, facilitating crack propagation and lowering fatigue strength [8]. The build rate is one key factor that significantly influences the manufacturing cost and is strongly dependent on process parameters such as laser power, scan strategy, scan speed, and layer thickness. These parameters control the thermal gradient of the melt pool and play a critical role in defect formation during L-PBF processing [18,19].

Fig. 3a shows the isopleth equilibrium diagram of tool steel. Austenite is more stable above 840°C, which transforms into ferrite and carbide precipitates during cooling. Due to the rapid thermal cycling of the laser processing (10^5-10^7 K s^{-1}), the as-built structure promotes martensite, with retained austenite within the martensite matrix (~ 10-15%). Formation of Cr-rich carbide occurs below 800°C without a distinct temperature range, while Mo-M_6C carbides rich in Mo form between 500-600°C [20]. Investigations by Zhang et al. [19] varied the scan speed and scan pattern to impose different thermal gradients in H13 steel, showing that these gradients govern the types and severity of defects that develop, and consequently the resulting fatigue behaviour. Specimens produced under the steepest thermal gradients exhibited microscopic solidification cracks caused by elemental segregation, along with centerline hot cracks, leading to the lowest matrix strength and fatigue performance. Although hot crack and solidification crack types are generally smaller than lack-of-fusion defects, they remain detrimental to mechanical performance. The specimens fabricated with the lowest thermal gradients showed moderate defect sizes, primarily spherical pores and vertical or horizontal cracks, and displayed the highest fatigue strength.

Fonseca et al. [21] examined the influence of laser power and scan speed on the microstructure along the interlayer and porosity formation. Among different test conditions, the microstructure remained largely consistent and was dominated by cellular/dendritic martensite with a significant fraction of retained austenite (16.5–29.7%). Fig. 3b shows the simplified schematic of the microstructure formation based on the temperature cycles. Temperatures above Ac3 result in the complete transformation to austenite and become martensite when cooling, with retained discontinuous austenite grains between martensite laths. Layer-by-layer thermal cycling induces intrinsic tempering, producing alternating fusion and heat-affected zones. At a higher solidification rate, the last to solidify layers do not contain massive carbide precipitates and are dominated by untempered martensite displaying higher hardness (552–614 HV). The bottom regions of the fusion zone showed the presence of precipitation with a dendritic/cellular structure. Heat-affected zones exhibited a degenerated or partially dissolved microstructure with more precipitates, resulting in lower hardness. The processing parameters in this scenario had a limited influence as the microstructure is strongly affecting consolidation quality.

Kisraoui et al. [22] investigated the influence of two printing strategies, bidirectional and chess scanning, combined with four-layer rotation angles (0°, 45°, 67°, and 90°), on the mechanical properties, hardness, and porosity of L-PBF processed H13 tool steel. The bidirectional strategy consistently outperformed the chess strategy, producing samples with lower porosity, higher relative density, and superior mechanical properties, whereas the chess strategy resulted in more severe defects, including extensive cracking and void formation, particularly at 45° and 67° rotations. As shown in Fig. 3c, a better homogeneity in the microstructure is achieved by consistent melt pool depth, macrostructure uniformity, and stable thermal profile. Higher elongation values ranging between 5.5-9% with better repeatability are noted for 67° rotational angle. The segmented scanning path and rapid thermal cycling inherent to the chess pattern mainly promoted elongated melt pool boundaries, intensifying thermal stresses, which are prone to brittle failure under tensile loading. Significant cracking is noted during printing due to residual stresses, which propagated along the melt pool boundaries and within the heat-affected zone. Fig. 3d shows the most common defects due to lack of fusion between the melt pools and solidification cracking formed during solidification across the melt pool [11]. Lack of fusion has been noted in samples with low-volumetric energy density (VED) where the neighbouring tracks did not melt, leading to a triangular void. Besides, gas pores

were noted in high VED, which is attributed to the vaporization effects because of their spherical morphology. The ratio of depth-to-width in L-PBF is influenced by power and speed, where lower speeds with higher power output can increase the depth of penetration. Higher scan speeds for a given power output could affect the penetration depth, and the optimal range for achieving good metallurgical bonding (2-3 layers) ranges from 0.3-0.6. Studies by Omidi et al. [23] showed that both size and number of porosities (keyhole and gas) increase for VED up to 57 J/mm^{3,} and lack of fusion was eliminated at this threshold. At 59 J/mm^3, keyhole porosities were absent and gas pores were evenly distributed, which is referred to as the "safe zone". However, when VED is increased above 61 J/mm^{3,} large keyholes form and lead to the reduction in the relative density of the part. The effect of VED on the porosity formation is shown in Fig. 3e. A higher volumetric energy density promotes the formation of a dense microstructure in L-PBF H13 steel, which is essential for achieving high thermal conductivity properties.

Effects of heat treatment and substrate preheating

As-built L-PBF H13 steels typically show poor ductility, prompting efforts to improve their mechanical performance through post-processing heat treatment. Heat treatments generally transform the retained austenite into martensite. While comparing post-treatment protocols, a single hardening followed by double-tempering treatment resulted in recrystallized grains, lath-type martensite, and the precipitation of fine spherical carbides along the boundaries of martensite laths. A double-tempering treatment at 550°C promotes precipitation of fine spherical carbides along the boundaries with the highest tensile strength of 2100 MPa, however, increasing the double-tempering treatment temperature to 650°C increases the sub-grain size and continuous network of carbide layers along with primary austenitic grain boundaries, promoting the ductility [20].

Table 1 Heat treatments on the microstructure and mechanical properties of H13 tool steels.

Heat treatment	Tensile strength (MPa)	Elongation (%)	Micro hardness (HV)	Comments on the microstructure observation	Ref
H13 AB	1900	9.7%	593	α-martensite matrix with 18.6% retained austenite (RA)	[20]
DT at 550°C	2100	7.6%	665	Promotes fully tempered martensite formation and precipitation of fine carbides	
DT at 650°C	1410	10.2%	485	Leads to carbide coarsening, recovery, recrystallization and stress relaxation	
SH at 1040°C + DT at 550°C	1450	9.2%	532	Fully tempered martensite formation and fine carbides distributed along the martensite lath boundaries and the prior austenite grain boundaries.	
H13 AB	2035	12.5	569	α-martensite matrix with 14.1% RA along with the precipitation of coarse VC (70.7 nm), and Fe_3C carbides	[24]
DT at 550°C	2265	7.8	652	Promotes fully tempered martensite formation, α-martensite grain coarsening, disappearance of Fe_3C and refinement of VC (23.8 nm)	

H13 AB	-	-	563	Typical α-martensite and RA with tensile residual stress of +34 MPa (measured from XRD using Cos(a) method)	[25]
DT at 550°C			480	Moderate effect on AB microstructure with the highest compressive residual stress of -957 MPa	
DT at 650°C			665	Precipitation of carbides with compressive residual stress of -573 MPa	
SH at1030°C+ T at 550°C			368	Clear outlines of α-martensite grains with the lowest compressive residual stress of -87 MPa	
SH at1030°C +T at 650°C			573	Enhanced precipitation of carbides with compressive residual stress of -265 MPa	
H13 AB with VED 63.7 J/mm^2		-		α-martensite matrix with RA	[26]
SH at 1020°C + DT at 495°C	1581	21%	496	Precipitation of fine secondary chromium-rich $M_{23}C_6$, VC, and molybdenum-rich M_6C carbides	
SH at 1020°C + DT at 550°C	1484	18.8%	291	Carbide coarsening	
SH at 1020°C + DT at 605°C	1309	20%	313	Precipitation of chromium-rich, stable M_7C_3 carbides	
H13 AB	1832 (25°C) 188 (600°C)	10.6% (25°C) 10.5% (600°C)	-	The retained austenite transforms into fresh martensite or decomposes into fine carbides at high temperature testing	[27]
DT at 495°C	1945 (25°C) 254 (600°C)	9.4% (25°C) 11.6% (600°C)		Better thermal stability due to finer carbides	
SH at 1020°C + DT at 495°C	1547 (25°C) 87 (600°C)	15.6% (25°C) 21.5% (600°C)		Carbide coarsening and matrix softening	

Note: AB- As-built, DT-double tempering, SH- solution hardening

In the as-built state, the microstructure of H13 consists of lath-type martensite and retained austenite within the martensitic regions. The percentage of retained austenite is higher (17%) for low energy density (75 J/mm3) and reduces to nearly 6% when the energy density is increased to 85 J/mm3, exhibiting exceptionally high strength of 2 GPa and hardness of 540–600 HV, along with moderate ductility (8.4–10%). Following post-build tempering at 650°C, the microstructure transforms into tempered martensite with finely dispersed carbides. Although this heat treatment leads to a reduction in strength, it significantly enhances ductility (15–16%), yielding mechanical performance comparable to that of conventionally processed H13 [19]. Quenching followed by double-tempering has been shown to increase thermal conductivity by up to 12%, as re-austenitization

eliminates the melt-pool structure and its associated boundaries, thereby reducing thermal resistance. This improvement, however, comes at the cost of reduced mechanical strength [28]. Yan et al. [29] demonstrated that optimising the tempering temperature can further improve strength–ductility combinations. As-printed H13 exhibited a yield strength of 818 MPa and an elongation of 2.42%, reflecting a brittle microstructure. Tempering at 600°C and 700°C improved their ductility to 5.8% and 10.9%, respectively. However, in terms of microstructure, 600°C tempering treatment exhibited a tempered martensitic matrix and dense precipitation of fine V-rich carbides, improving yield strength to 1483 MPa. Meanwhile, the microstructure of 700°C tempered H13 coarsened the carbide precipitates, thus relatively lowering the yield strength to 877 MPa. Table 1 summarizes some recent notable works on the effects of heat treatments with microstructural observations.

Preheating of the substrate has been identified as an effective strategy for mitigating residual stresses in AM components. Elevated residual stresses, together with a higher carbide fraction, can increase susceptibility to crack initiation and propagation under thermal loading conditions [18]. Preheating temperatures below 200°C promote horizontal cracking, while temperatures between 200 and 600°C are identified as the crack-free processing range [11]. Zong et al. [30,31] investigated the effect of preheating temperature at 200°C and 500°C during L-PBF processed H13 steel. Higher preheating temperature affects the molten pool geometry by increasing the average depth and width, promoting epitaxial growth, carbide precipitation in the cell boundaries, and reducing the number of pores along the build direction. Bainitic transformation is promoted for preheating at 500°C, while the low preheating samples are still dominated by martensite microstructure (200°C) [30]. When fabricated at a preheating temperature of 200°C, variations in build orientation (horizontal (H13-200H) and vertical (H13-200V)) did not result in significant differences in tensile strength and elongation (Fig. 4a). In contrast, a noticeable variation in these mechanical properties is observed for H13 specimens produced using a strip scan strategy with a 61° rotation angle, even under the same preheating conditions. This indicates that differences in scan strategy and processing parameters can have a more pronounced effect on mechanical performance than build orientation and preheating temperature. Fractographic analysis (Fig. 4b) further reveals that the improved properties of H13-200V specimens are associated with reduced defect populations and fracture behaviour governed by martensitic lath structures [26]. Although porosities are present in the samples, a mixed fracture mode can be seen where the fracture is controlled by microstructure rather than the defects.

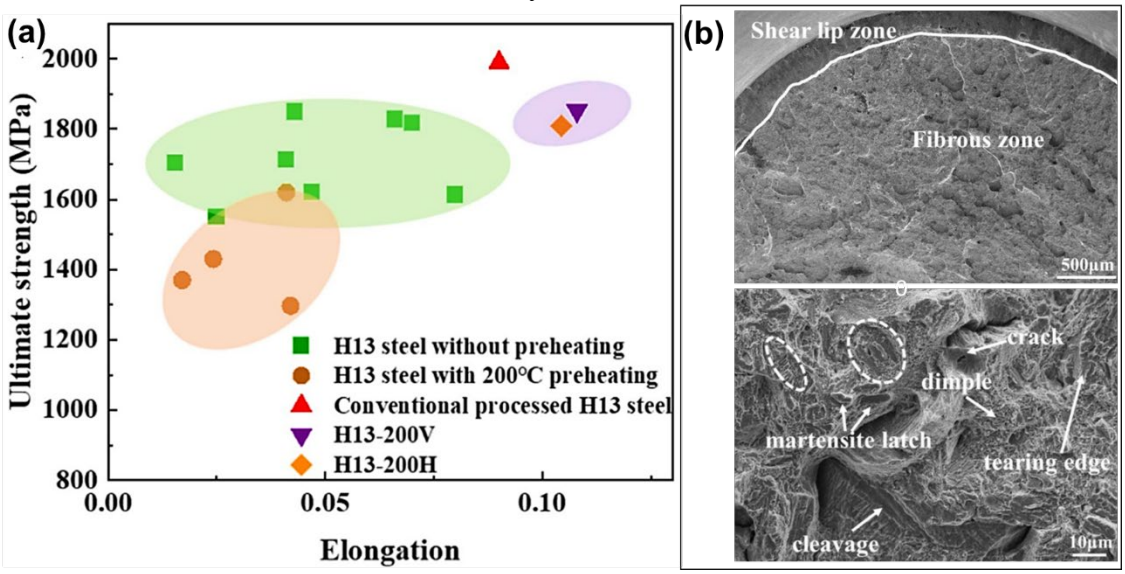

Fig. 4 (a) Mechanical property comparison of conventional and LPBF-processed H13 steel and (b) fracture surface of H13 vertically built on preheated substrate at 200°C *[31]*.

For AM processing, it is critical to understand the role of the preheating and post-heat treatment process, which generally produces secondary carbide precipitation, shifting the secondary hardening peak, and converting tensile stresses into beneficial compressive stress, improving the overall ductility for tooling applications [32].

AM inserts for conformal cooling of dies in HPDC applications

Direct metal additive process is highly attractive for tool building process due to rapid response time to market, enabling tooling functionalization and higher performance, although the process chain involves standard processes including machining, thermal treatments, grinding, and polishing. A much-valued advantage is the fabrication of conformal cooling channels for molds used in both plastic injection and metallic materials as an alternative to the deep drilled straight channel cooling system. Conformal cooling channels match the design of the mold cavity (equidistant from the mold surfaces) mostly with variable and non-circular cross sections with additional design features such as fins, helical, or lattice structures [13]. The efficiency of the cooling channels is determined by several factors including the type of channels (circular, ellipsoid or others), layout (spiral, mesh, vascularized), placement, location of adjacent channels, and other modular aspects considered either in design or in construction (lattice structures) [13].

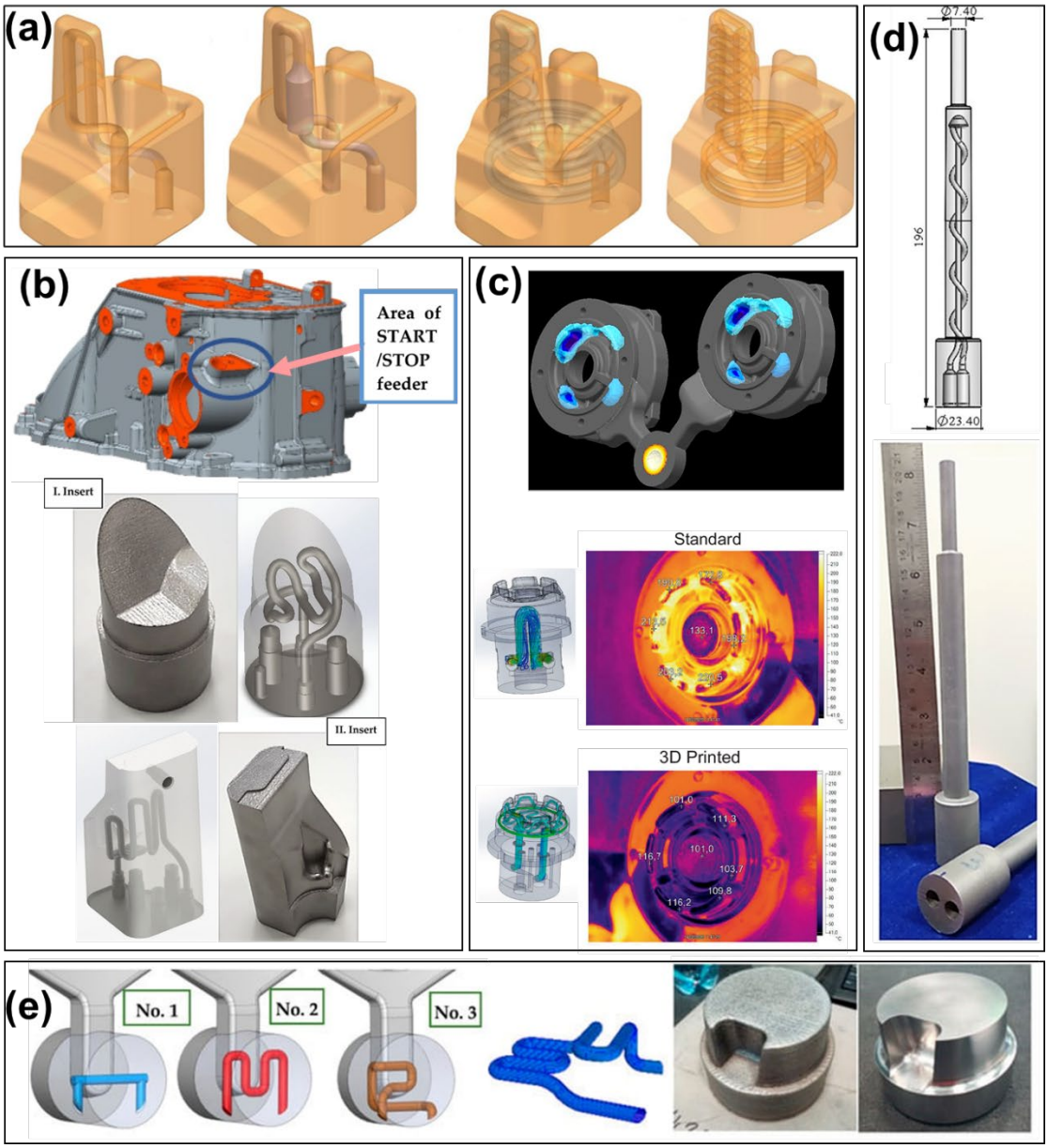

Fig. 5 (a) Different designs of conformal cooling inserts *[34]*, conformal cooling HPDC inserts for (b, c) gear box housings *[35,36]*, (d) core pin *[32]*, and (e) metal diffuser at the gating system *[37]*.

Modelling results suggest that enhanced thermal management can extend die life from approximately 80,000 to at least 120,000 cycles, a 50% improvement that offers clear benefits for high-volume manufacturing. Improved thermal control also helps eliminate hot spots and reduce

shrinkage porosity, leading to better part quality and a potential reduction in scrap rate from 5% to 3%. Collectively, these gains can lower unit production costs by up to 10%, representing a meaningful advancement toward both economic and sustainability benefits [33]. Different geometries of cooling channels with a single loop, a single loop with a larger diameter, a single spiral loop, and a bi-directional spiral loop are investigated for the cooling performance, pressure drop, stress, and failure life by He et al. [34] (Fig. 5a). Overall, single-spiral and bi-directional spiral loops showed the lowest thermal gradient and reduced risk of vapour bubble formation using simulations; however, the propensity of fabrication defects is not discussed for all designs.

Fig. 5b shows the application of a conformal cooling insert to the MQ 200 GA gearbox housing reported by Andronov et al. [36]. Pressure test revealed that a significant number of parts failed due to the defect in the START/STOP feeder area. Simulation of solidification has shown that the last to solidify metal is located directly inside the feeder (with a shrinkage volume of 0.186 cm^3) in which either the continuous feeding is restricted or no heat dissipation is in place. To address this issue, a conformal cooling insert (MS1 maraging steel) was designed and printed using the L-PBF process as shown in Fig. 5b. During the test series of 8000 casting cycles, the pressure test indicated that the acceptable number of parts increased to 92%, shrinkage pore volume reduced by 6%, and produced nearly 43000 castings before showing signs of wear. This study also demonstrated that the simulation tools are more reliable in predicting the temperature field verified by thermal camera imaging.

Fig. 5c addresses the issue of section thickness affecting the cooling rate in the HPDC process using conformal cooling of molds. It has been shown that the highest temperature detected after 5 cycles for conformally cooled die insert is ~104°C lower than the traditional die. In addition, the duration of positioning and blowing is reduced, die cooling time and solidification time were faster, contributing to the overall cycle time improvement by 11%. The AM fabricated die tested for different sprinkling oil temperatures for 15000 cycles showed that highly loaded areas of the casting had slightly fewer defects compared to the standard die [35]. For an engine crank case produced by HPDC process, Karakoc et al. [38] reported the effect of conformal cooling on porosity reduction, die surface temperature, and microstructure. Simulation results indicated that the peak die surface temperature without cooling is in the range of 350-370°C, which is reduced to 310-340°C with conformal cooling (before lubrication). This reduces the lubrication time from 4 s for the traditional mold to 2 s after employing conformal cooling. Dendritic size refinement, porosity size reduction (251 to 156 mm^3 and 108 to 91 mm^3) were noted in two locations of the casting after conformal cooling, although the porosity could not be eliminated completely.

Similarly, a Zamak alloy fabricated using a conformally cooled die in the HPDC process offers a 50% reduction in surface defects for the same level of spray lubrication, decrease in cycle time, and shrinkage porosity volume. The redesigned insert was used in the production cycles for nearly 200 cycles without any damage due to wear [39]. Fig. 5d shows a case study of HPDC core pin that demonstrated the practical benefits of AM fabricated die parts. The SLM built pin, incorporating a 2.5 mm internal cooling channel, achieved a 15–20% reduction in surface temperature compared to the conventional, non-cooled design. This improved thermal management shortened the casting cycle time by 2 seconds and reduced surface porosity in the cast parts, leading to fewer rejections. Fig. 5e demonstrates the application of conformal cooling to the metal diffuser at the gating system that typically experiences a pressure of 70 MPa and metal flow speeds of 30-40 m/s. A stress threshold is adopted (400 MPa at 400°C and 600 MPa at 600°C) to analyse the variation of cyclic stresses of the designs numerically. Design No 3 offered better performance of all; interestingly, design No 2 has large fluctuation of stresses from 300 to 700 MPa, while the stresses in traditional design 1 are stable at 500 MPa. It has been highlighted that often a cooling channel designed closer to mold surfaces could enhance cooling; however, large gradients over a short distance could lead to earlier failure [37]. All these results demonstrate that the industrial readiness of conformally cooled AM tooling for HPDC applications [32]. It should be highlighted that the cooling enables faster cycle time, whereas more analysis is required to assess the component thickness, filling speed required, distance from the insert surface, and numerical simulations to verify adequate feeding. For instance, semi-solid HPDC

provided similar benefits to that of the conformal cooling; however, the use of conformal cooling with semi-solid metals exhibits difficulties to fill and porosities in the casting [14].

Geometrical constraints and surface roughness of the cooling channels are very important for better performance over a longer period. Typically, large overhangs and build angles less than 45° require support structures. It has been reported that the cooling channels fabricated above 10 mm led to failure by collapsing where support structures are essential (Fig. 6a). Cooling channel with supporting structures inside facilitates the manufacturability of cooling channels with diameters greater than 10 mm until 20 mm; however, for reduced internal struts, thickness below 4 mm causes fracturing due to poor fusion and residual stresses. A 20% reduction in cooling time has been observed for a 13 mm strut design compared to an 8 mm cooling channel without any supporting structures [40].

Fig. 6b shows the corrosion and crack formation of the single loop cooling channel. Cracks formed from inside the conformal cooling channel and areas undergoing corrosion are identified by the presence of grooves and strips. Extended exposure to coolant and vapour formation is the main reason for the strip formation. The presence of line distribution of pores during the fabrication stage due to gas or vaporisation of powders could act as weak sites for crack initiation and propagation. In addition, pores present in molten pool boundaries can also act as weak sites for crack propagation and coolant leakage [34]. Failure of an HPDC insert fabricated using 18Ni300 maraging steel is shown in Fig. 6c. The insert operated with water at 150°C and 5.25 bar and failed within ~15000 cycles, which is very short compared to a typical HPDC service life. Detailed analysis indicated that the cracks preferentially initially from the channel edges, where a combination of thermo-mechanical stresses during operation and defects/residual introduced during the fabrication process are also stated as possible sources. Since most of the cracks propagated in a straight path, the probable mechanism could be stress-induced corrosion due to cyclic gradients rather than melt pool geometries or other process-induced factors [41]. Another important characteristic feature of AM processed cooling channels is the higher surface roughness, which on the one hand could promote heat transfer, while exhibiting inferior flowability (< 10 mm) especially when the flow becomes turbulent, leading to failures [42].

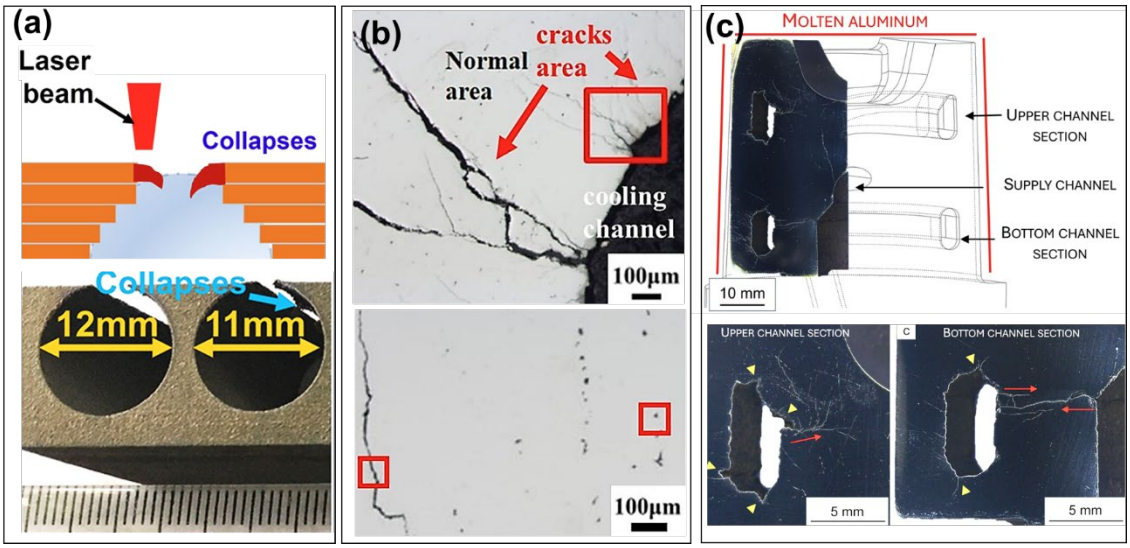

Fig. 6(a) Manufacturability analysis of AM fabricated cooling channel indicates the collapsing defect [40]. (b) Major cracks originating from the inner side of the cooling channels (1), crack propagation (2), and porosity areas (3) [34] and (c) cracking of a die HPDC insert (18Ni300 maraging steel) [41].

AM also enables die design concepts in bimetallic structures that are not achievable with conventional machining, allowing HPDC dies to be optimized for thermal management, durability, and functional integration. Copper is widely used for heat dissipation due to its high thermal conductivity of 402 W/m K. Incorporating a copper lining inside the cooling channels of the steel mold has been shown to improve the cooling rate by approximately 12% [43]. Three-dimensional

(3D) lattice composite structures can significantly broaden the spectrum of achievable thermal properties, creating new opportunities for designing multifunctional tool dies. For HPDC dies, which are subjected to extreme thermal loads, H13 lattice structures infiltrated with copper offer a promising route to produce dies that dissipate heat more efficiently, thereby enhancing both die performance and casting quality. Osman et al. [44] developed a two-step approach in which L-PBF was first used to fabricate functionally graded H13 lattice structures, followed by copper infiltration and quenching with double-tempering. L-PBF H13 structures featured an octet truss unit cell designed for load capacity and efficient heat transfer. The H13 volume fraction was graded from 40% at the top to 100% at the bottom. The as-built H13 exhibited a lath martensite microstructure with 16% retained austenite. Copper infiltration produced a nearly fully dense composite with excellent bonding between the steel and copper phases, while preserving the tempered H13 microstructure. The resulting composite exhibited highly tuneable thermal conductivity, ranging from 34 to 145 W/m K depending on the H13 volume fraction, which is significantly higher than the thermal conductivity typically reported for L-PBF fabricated H13 (22–24 W/m K [28,45]).

Asnafi [9] evaluated the use of laser-based AM, specifically L-PBF for manufacturing, surface treatment, and repair of tooling across cold-working, hot-working, and injection-molding applications. Compared to the mechanical properties of wrought H13 (yield strength of 1290-1570 MPa, and tensile strength of 1500-1600 MPa in hardened condition), AM exhibits a lot of variability due to the challenges in optimising process conditions for defect reduction and microstructure uniformity. This is also reflected in fatigue testing and other performance studies shown in Fig. 5 and Fig. 6 for cooling channels [15]. Functional enhancements to the die surface can enhance the performance; for instance, Ni-based cladding applied to an L-PBF maraging steel subs strate reduced friction by 25% and improved wear resistance by a factor of 45. Other ceramic reinforcements (carbides, borides, and oxides) or hard-facing with Co-based and Ni-based alloys can enhance resistance to high temperature, wear, and corrosion; however, the increased processing cost limits their broader applications [9].

Role of AM in die remanufacturing

Remanufacturing is a process of reworking the end-of-life product to be usable with its original or better performance as a newly manufactured product with warranty [9]. This involves a series of processing stages inducing disassembly, sorting and cleaning, inspection, reconditioning, reassembly and testing. This requires higher skills than the design of the original product as it involves multiple steps in dismantling, restoring, replacing, and testing individual and whole (assembled) components to validate the functionality of the remanufactured part. The key benefits of the remanufacturing process include effective resource management, reduction in the usage of materials and resources, lower emissions and energy usage, and provides significant opportunities for the development of skilled jobs and economic growth.

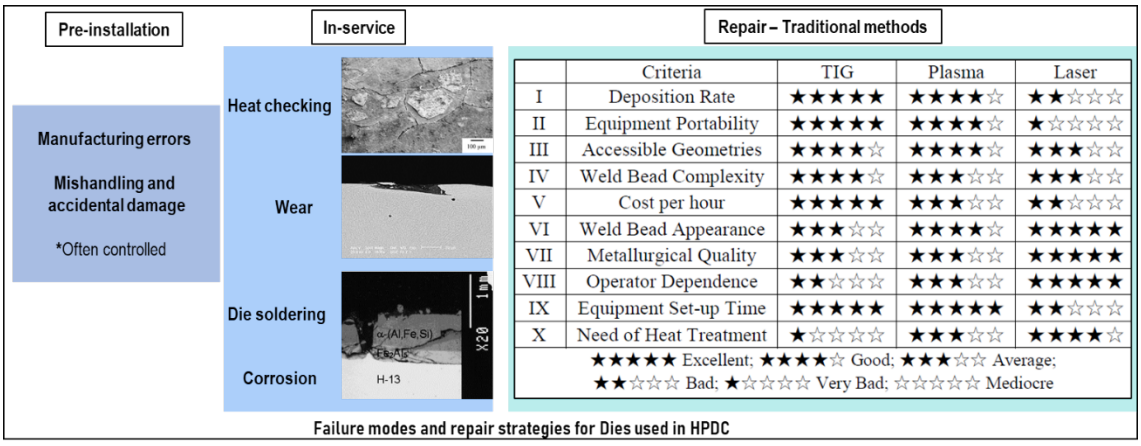

	Criteria	TIG	Plasma	Laser
I	Deposition Rate	★★★★★	★★★★☆	★★☆☆☆
II	Equipment Portability	★★★★★	★★★★☆	★☆☆☆☆
III	Accessible Geometries	★★★★☆	★★★★☆	★★★☆☆
IV	Weld Bead Complexity	★★★★☆	★★★☆☆	★★★☆☆
V	Cost per hour	★★★★★	★★★☆☆	★★☆☆☆
VI	Weld Bead Appearance	★★★☆☆	★★★★☆	★★★★★
VII	Metallurgical Quality	★★★☆☆	★★★☆☆	★★★★★
VIII	Operator Dependence	★★☆☆☆	★★★☆☆	★★★★★
IX	Equipment Set-up Time	★★★★★	★★★★★	★★☆☆☆
X	Need of Heat Treatment	★☆☆☆☆	★★★☆☆	★★★★☆

★★★★★ Excellent; ★★★★☆ Good; ★★★☆☆ Average;
★★☆☆☆ Bad; ★☆☆☆☆ Very Bad; ☆☆☆☆☆ Mediocre

Fig. 7 Common failure modes of HPDC dies and a summary of traditional methods employed in traditional repair works[6].

Fig. 7 shows the comparison of the most used welding technologies in die repair, where the selection of a particular process depends on various attributes such as cost, portability, set-up time, quality of the weld, and other considerations such as post-weld treatments. Laser-based techniques show superior metallurgical quality of the weld; however, as discussed in the above sections, the role of processing variables, residual stress, and martensite formation needs to be addressed [6].

Compared to original manufacturing, remanufacturing requires more skills and competency to determine the worthiness of the component. This includes accessibility of the damage, volume, shape, and machinability considerations after remanufacturing. Generally, the process of remanufacturing starts with pre-machining of damaged parts, where the worn-out surfaces or heat checks and corroded surfaces are removed prior to AM. Secondly, based on the type of defects (surface impact defect or superficial cracking), a reverse engineering approach can be used to generate the damaged surface from which the undamaged surface will be reconstructed [46]. Remanufacturing of casting dies holds significant value retention, boosts productivity, and enables circular manufacturing in foundries; however, establishing a remanufacturing pathway is more complex as it relies on operator skills.

Summary and Prospects

Extending die life is crucial for the productivity of the die casting industry, especially in HPDC and ultra-large castings, as it boosts productivity and supports circular manufacturing practices in foundries. Laser powder bed fusion process provides several key benefits in terms of manufacturability, microstructure, and mechanical properties of H13 dies used in HPDC process. In particular, conformal cooling die-inserts gained significant industry interest for increased die life, which otherwise seems difficult to achieve with conventional manufacturing processes. Reduction in the size of shrinkage porosities, lubricant usage, core temperature, cycle time, and stabilizing thermal fields are key benefits of die inserts. Best practices for producing AM parts with reproducible properties require a complete understanding of processing variables (powder quality, laser variable, and machine variables) to achieve high density as-built parts, followed by post-processing heat treatment to improve the microstructure homogeneity, residual stress reduction, and precipitate formation. Preheating treatment has also been shown to reduce residual stresses, a fraction of retained austenite, and solidification cracking. Integration of AM into die remanufacturing offers significant cost benefits, along with additional opportunities for functional improvements (such as conformal cooling and laser surface treatments), compared to complete die replacement in case of failure. Nevertheless, significant challenges lie ahead to achieve successful integration of AM in die applications for longer service life.

(i) The primary challenge lies within the fabrication step where the role of processing variables and factors causing variability within the process needs to be established. The importance of preheating to control microstructure and cracking, and post-processing heat treatment to reduce residual stresses is evident. Understanding the effect of machine variables, strategies of printing and controlling their interdependencies could reduce variability in the results due to porosities (lack of fusion or keyhole pores), cracking, and as-built microstructure. Data reported in the literature are often incomparable due to the inconsistency in methodologies and procedure.

(ii) The second level of challenge lies in the testing of AM parts produced in the actual production environment, for both insert and remanufactured parts. Numerical simulation studies for topology optimization, testing under controlled conditions reveal promising results for die inserts (reducing the cycle time, lubrication time, peak temperatures and stresses); however, longer testing duration and follow-up studies on the failure mechanisms are essential. While this review is limited by the data available in such studies, only a few studies have stated that failure of conformal cooling channels before the expected lifetime of the die. In some cases, it has been stated that there is no conclusive evidence on whether processing defects or operational defects caused failure. Therefore, more standardization of tests and research work is needed in this regard.

References

[1] A. Rolseth, M. Carlson, E. Ghassemali, L. Pérez Caro, A.E.W. Jarfors, Impact of functional integration and electrification on aluminium scrap in the automotive sector: A review, Resources, Conservation and Recycling 205 (2024) 107532. https://doi.org/10.1016/j.resconrec.2024.107532.

[2] D. Lehmhus, Advances in Metal Casting Technology: A Review of State of the Art, Challenges and Trends—Part I: Changing Markets, Changing Products, Metals 12 (2022) 1959. https://doi.org/10.3390/met12111959.

[3] G. Roberts, G. Krauss, R. Kennedy, Selection of Tool Steels, in: Tool Steels, 5th ed., ASM International, Ohio, 2000: pp. 7–29.

[4] C. Chen, Y. Wang, H. Ou, Y. He, X. Tang, A review on remanufacture of dies and moulds, Journal of Cleaner Production 64 (2014) 13–23. https://doi.org/10.1016/j.jclepro.2013.09.014.

[5] P. Solgi, M. Chenarani, A.R. Eivani, M. Ghosh, V. Kumar, H.R. Jafarian, Heat checking as a failure mechanism of dies exposed to thermal cycles: A review, Journal of Materials Research and Technology 26 (2023) 865–895. https://doi.org/10.1016/j.jmrt.2023.07.170.

[6] C.R. Chen, Y. Wang, H.A. Ou, N. Gindy, Remanufacture of Die Casting Dies, AMM 121–126 (2011) 3482–3486. https://doi.org/10.4028/www.scientific.net/AMM.121-126.3482.

[7] C.-D. Li, H.-Y. Yang, B.-X. Dong, D.-L. Chen, S.-L. Shu, F. Qiu, Q.-C. Jiang, L.-C. Zhang, Thermal fatigue failure mechanisms and enhancement strategies of die steel, Journal of Materials Research and Technology 38 (2025) 4567–4599. https://doi.org/10.1016/j.jmrt.2025.08.198.

[8] J. Lee, J. Choe, J. Park, J.-H. Yu, S. Kim, I.D. Jung, H. Sung, Microstructural effects on the tensile and fracture behavior of selective laser melted H13 tool steel under varying conditions, Materials Characterization 155 (2019) 109817. https://doi.org/10.1016/j.matchar.2019.109817.

[9] N. Asnafi, Tool and Die Making, Surface Treatment, and Repair by Laser-based Additive Processes, Berg Huettenmaenn Monatsh 166 (2021) 225–236. https://doi.org/10.1007/s00501-021-01113-2.

[10] H. Fayazfar, M. Salarian, A. Rogalsky, D. Sarker, P. Russo, V. Paserin, E. Toyserkani, A critical review of powder-based additive manufacturing of ferrous alloys: Process parameters, microstructure and mechanical properties, Materials & Design 144 (2018) 98–128. https://doi.org/10.1016/j.matdes.2018.02.018.

[11] L. Wu, S. Das, W. Gridin, S. Leuders, M. Kahlert, M. Vollmer, T. Niendorf, Hot Work Tool Steel Processed by Laser Powder Bed Fusion: A Review on Most Relevant Influencing Factors, Adv Eng Mater 23 (2021) 2100049. https://doi.org/10.1002/adem.202100049.

[12] S. Arman, I. Lazoglu, A comprehensive review of injection mold cooling by using conformal cooling channels and thermally enhanced molds, Int J Adv Manuf Technol 127 (2023) 2035–2106. https://doi.org/10.1007/s00170-023-11593-w.

[13] S. Feng, A.M. Kamat, Y. Pei, Design and fabrication of conformal cooling channels in molds: Review and progress updates, International Journal of Heat and Mass Transfer 171 (2021) 121082. https://doi.org/10.1016/j.ijheatmasstransfer.2021.121082.

[14] A.E.W. Jarfors, R. Sevastopol, K. Seshendra, Q. Zhang, J. Steggo, R. Stolt, On the Use of Conformal Cooling in High-Pressure Die-Casting and Semisolid Casting, Technologies 9 (2021) 39. https://doi.org/10.3390/technologies9020039.

[15] N. Omidi, P. Farhadipour, L. Baali, K. Bensalem, N. Barka, M. Jahazi, A Comprehensive Review of Additively Manufactured H13 Tool Steel Applicable in the Injection Mold Industry: Applications, Designs, Microstructure, Mechanical Properties, JOM 75 (2023) 4457–4469. https://doi.org/10.1007/s11837-023-05735-4.

[16] O. Zinovieva, V. Romanova, E. Dymnich, A. Zinoviev, R. Balokhonov, A Review of Computational Approaches to the Microstructure-Informed Mechanical Modelling of Metals Produced by Powder Bed Fusion Additive Manufacturing, Materials 16 (2023) 6459. https://doi.org/10.3390/ma16196459.

[17] W.K. Law, K.-C. Wong, H. Wang, Z. Sun, C.S. Lim, Microstructure Evolution in Additively Manufactured Steel Molds: A Review, J. of Materi Eng and Perform 30 (2021) 6389–6405. https://doi.org/10.1007/s11665-021-05948-1.

[18] D.M. Santhoshsarang, S. Narayanaswamy, G. Telasang, K. Divya, R. Bathe, G.L. Samuel, Additive Manufacturing of AISI H13 Tool Steel with Combinations of Higher Laser Power and Scan Speed: Microstructural and Mechanical Properties Insights, J. of Materi Eng and Perform 34 (2025) 17491–17502. https://doi.org/10.1007/s11665-024-10467-w.

[19] J. Zhang, J. Schumacher, B. Clausen, A comprehensive study on the influence of the scan pattern in two porosity levels and surface roughness on the fatigue behavior of laser powder bed fusion manufactured specimens made of steel H13, J Mater Sci 58 (2023) 10457–10483. https://doi.org/10.1007/s10853-023-08541-0.

[20] H. Hosseinlou, M. Shakeri, A.W. Abdelghany, M. Jaskari, A. Järvenpää, A. Hamada, Tailoring microstructure and mechanical properties of additively manufactured H13 tool Steel: Influence of build orientation and tempering treatments, Materials Science and Engineering: A 942 (2025) 148708. https://doi.org/10.1016/j.msea.2025.148708.

[21] E.B. Fonseca, A.H.G. Gabriel, L.C. Araújo, P.L.L. Santos, K.N. Campo, E.S.N. Lopes, Assessment of laser power and scan speed influence on microstructural features and consolidation of AISI H13 tool steel processed by additive manufacturing, Additive Manufacturing 34 (2020) 101250. https://doi.org/10.1016/j.addma.2020.101250.

[22] C. Kisraoui, N. Omidi, S. Dehghan, A. Belhadj, S. Slama, N. Barka, A. El Ouafi, Effect of Printing Strategies on Mechanical Properties of Tool Steel in Laser Powder Bed Fusion Process, Lasers Manuf. Mater.Process. 12(2025)147-173. https://doi.org/10.1007/s40516-025-00275-y.

[23] N. Omidi, M. Houria, M.M. Monjez, M. Jahazi, N. Barka, A.E. Ouafi, Processing parameters optimization for enhanced mechanical strength in PBF-ed H13 tool steel: minimizing manufacturing defects including microstructural inhomogeneity, sub-surface porosities, and oxide formation, Int J Adv Manuf Technol 136 (2025) 2681–2706. https://doi.org/10.1007/s00170-024-14951-4.

[24] F. Yu, X. Yu, Y. Pan, D. Zhang, Tailoring strength-ductility balance in laser powder bed fusion H13 steel via intrinsic heat treatment-induced heterostructure and tempering homogenization, Materials Science and Engineering: A 952 (2026) 149671. https://doi.org/10.1016/j.msea.2025.149671.

[25] F.F. Conde, E.B. Fonseca, S.A. Freire, É.S.N. Lopes, Impact of Heat Treatments on Residual Stress in Additively Manufactured AISI H13 Tool Steel, J. of Materi Eng and Perform 34 (2025) 29977–29987. https://doi.org/10.1007/s11665-025-11522-w.

[26] M.M. Monjez, N. Omidi, P. Farhadipour, N. Barka, A.E. Ouafi, Process-structure–property relationships in laser powder bed fusion of H13 tool steel: effect of processing and tempering conditions on microstructure and mechanical properties, Int J Adv Manuf Technol 139 (2025) 2481–2504. https://doi.org/10.1007/s00170-025-16024-6.

[27] M.M. Monjez, N. Omidi, P. Farhadipour, A. El Ouafi, N. Barka, Influence of Different Heat Treatments on Microstructure Evolution and High-Temperature Tensile Properties of LPBF-Fabricated H13 Hot Work Steel, Metals 15 (2025) 1003. https://doi.org/10.3390/met15091003.

[28] Y. Sun, J. Wang, M. Li, Y. Wang, C. Li, T. Dai, M. Hao, H. Ding, Thermal and mechanical properties of selective laser melted and heat treated H13 hot work tool steel, Materials & Design 224 (2022) 111295. https://doi.org/10.1016/j.matdes.2022.111295.

[29] J. Yan, H. Song, Y. Dong, W.-M. Quach, M. Yan, High strength (~2000 MPa) or highly ductile (~11%) additively manufactured H13 by tempering at different conditions, Materials Science and Engineering: A 773 (2020) 138845. https://doi.org/10.1016/j.msea.2019.138845.

[30] H. Zong, N. Kang, M. El Mansori, Impact of applied loads on wear mechanisms in H13 steel at various preheating temperatures during laser powder bed fusion additive manufacturing, Wear 556–557 (2024) 205538. https://doi.org/10.1016/j.wear.2024.205538.

[31] H. Zong, N. Kang, M. El Mansori, Characterizations of the anisotropic features of the phase, texture and deformation behavior of laser powder bed fusion-processed H13 steel, Materials Characterization 228 (2025) 115403. https://doi.org/10.1016/j.matchar.2025.115403.

[32] D.M. Santhoshsarang, K. Divya, G. Telasang, S. Soundarapandian, R. Bathe, G. Padmanabham, Additively Manufactured High-Performance Conformally Cooled H13 Tool Steel Die Insert for Pressure Die Casting, Trans Indian Natl. Acad. Eng. 6 (2021) 1037–1048. https://doi.org/10.1007/s41403-021-00233-y.

[33] H. Jacob Roos, M. Lagler, L. Quintana, The Future of Structural Components in HPDC-Taking die-cast structural components into the mass automotive market, Bühler Die Casting, n.d.

[34] X. He, X. Wang, C. Vian, M. Faezipour, Numerical optimization of conformal cooling channels for thermal distribution and stress characterization in additively manufactured high pressure die casting die, Engineering Failure Analysis 176 (2025) 109620. https://doi.org/10.1016/j.engfailanal.2025.109620.

[35] P. Barreiro, G. Armutcu, S. Pfrimmer, J. Hermes, Quality improvement of an aluminum gearbox housing by implementing additive manufacturing, Forsch Ingenieurwes 86 (2022) 605–616. https://doi.org/10.1007/s10010-021-00541-3.

[36] V. Andronov, Z. Pitrmuc, J. Zajíc, P. Šotka, L. Beránek, M. Bock, Conformal cooling as a support tool for eliminating local defects in high-pressure die casting series production, Prog Addit Manuf 10 (2025) 1511–1528. https://doi.org/10.1007/s40964-024-00721-x.

[37] M. Małysza, R. Żuczek, D. Wilk-Kołodziejczyk, K. Jaśkowiec, A. Bitka, M. Głowacki, Ł. Zięba, S. Pysz, Application of a 3D-Printed Part with Conformal Cooling in High-Pressure Die Casting Mould and Evaluation of Stress State During Exploitation, Materials 17 (2024) 5988. https://doi.org/10.3390/ma17235988.

[38] C. Karakoc, K.C. Dizdar, D. Dispinar, Investigation of effect of conformal cooling inserts in high-pressure die casting of AlSi9Cu3, Int J Adv Manuf Technol 121 (2022) 7311–7323. https://doi.org/10.1007/s00170-022-09808-7.

[39] A. Armillotta, R. Baraggi, S. Fasoli, SLM tooling for die casting with conformal cooling channels, Int J Adv Manuf Technol 71 (2014) 573–583. https://doi.org/10.1007/s00170-013-5523-7.

[40] C. Tan, D. Wang, W. Ma, Y. Chen, S. Chen, Y. Yang, K. Zhou, Design and additive manufacturing of novel conformal cooling molds, Materials & Design 196 (2020) 109147. https://doi.org/10.1016/j.matdes.2020.109147.

[41] L. Marchini, M. Gelfi, L. Solazzi, A. Pola, Root-Cause Analysis of a Failed LPBF Conformal Cooling Insert for Die Casting, Inter Metalcast (2025). https://doi.org/10.1007/s40962-025-01806-1.

[42] M. Sode, M. Kahlert, T. Arold, A.P. Fros, M. Vollmer, T. Niendorf, M. Fehlbier, Tailoring flow behavior and heat transfer in tempering channels for high-pressure die casting—analysis of potentials of commercial static mixers and prospects of additive manufacturing, Int J Adv Manuf Technol 125 (2023) 5463–5477. https://doi.org/10.1007/s00170-023-10920-5.

[43] S.-S. Shin, S.-K. Lee, D.-K. Kim, B. Lee, Enhanced cooling channel efficiency of high-pressure die-casting molds with pure copper linings in cooling channels via explosive bonding, Journal of Materials Processing Technology 297 (2021) 117235. https://doi.org/10.1016/j.jmatprotec.2021.117235.

[44] M. Osman, P. Wanjara, J. Gholipour, F. Bernier, M. Molavi-Zarandi, M. Brochu, H13 tool steel-copper composite fabricated by laser powder bed fusion and melt infiltration for high thermal conductivity tooling applications, Materials Today Communications 49 (2025) 114221. https://doi.org/10.1016/j.mtcomm.2025.114221.

[45] J. Džugan, K. Halmešová, M. Ackermann, M. Koukolíková, Z. Trojanová, Thermo-physical properties investigation in relation to deposition orientation for SLM deposited H13 steel, Thermochimica Acta 683 (2020) 178479. https://doi.org/10.1016/j.tca.2019.178479.

[46] X. Zhang, W. Cui, W. Li, F. Liou, A Hybrid Process Integrating Reverse Engineering, Pre-Repair Processing, Additive Manufacturing, and Material Testing for Component Remanufacturing, Materials 12 (2019) 1961. https://doi.org/10.3390/ma12121961.